

Local Trajectory Planning For UAV Autonomous Landing

Yossi Magrisso, Ehud Rivlin and Hector Rotstein

Abstract—An important capability of autonomous Unmanned Aerial Vehicles (UAVs) is autonomous landing while avoiding collision with obstacles in the process. Such capability requires real-time local trajectory planning. Although trajectory-planning methods have been introduced for cases such as emergency landing, they have not been evaluated in real-life scenarios where only the surface of obstacles can be sensed and detected. We propose a novel optimization framework using a pre-planned global path and a priority map of the landing area. Several trajectory planning algorithms were implemented and evaluated in a simulator that includes a 3D urban environment, LiDAR-based obstacle-surface sensing and UAV guidance and dynamics. We show that using our proposed optimization criterion can successfully improve the landing-mission success probability while avoiding collisions with obstacles in real-time.

Index Terms—Trajectory planning, Autonomous landing

I. INTRODUCTION

Providing autonomous features to UAVs is of major importance. Autonomy can free human operators from flight tasks, reduces the dependency on wireless communication, and also increases the number of platforms operating safely and simultaneously in a given area. Among other important autonomous features, navigation, obstacle collision avoidance and landing sites exploration are of interest in the present work. Having these features can enable solving the “last mile” problem for package delivery or for applications requiring provisions for emergency landing [7].

When performing an autonomous mission, a UAV will usually execute a global path, pre-calculated to be optimal for some significant performance criterion. As opposed to this, a *Local Trajectory planner* (LTP) has the objective of calculating and executing a local path that attempts to follow the global path as close as possible while avoiding collision with obstacles that were not considered in the pre-computations [4]. A local Planner has to be efficient since it needs to run in soft real-time and possibly recalculate the trajectory whenever a new obstacle is detected. However, optimizing the trajectory to some extent is most desirable.

A risk-based trajectory planning approach was introduced in [17, 18]. In this work a risk map is used as an input for the optimization process, and a modification of the optimal A^* algorithm [6], namely $riskA^*$, is used for planning a trajectory

that minimizes the risk when flying over populated areas. This approach can be adopted for the autonomous landing site search, with a difference of using an *opportunity* map instead of a risk map.

For obstacle collision avoidance LTP algorithms usually require minimal a-priori information of the environment since sensor-based data is more relevant and important. For instance, the bio-inspired Bug family of algorithms [15, 11] plan local trajectory in the continuous configuration space by following a direct path to the goal point while bypassing obstacles along their surface border whenever they are encountered. More aggressive success-oriented methods attempt to find local trajectories by using optimized Hermite polynomials [14] or Bézier curves [9, 3, 1, 10, 4]. The optimization criteria can include minimizing length, curvature, time-of-flight, or energy consumption, or maximizing smoothness and consistency. Although these algorithms work well in some cases, they are neither optimal nor complete.

Realistic obstacle detection and mapping must be taken into account when evaluating performance of trajectory-planning algorithms. Most sensors can sense and map only the outer surfaces of obstacles but not their interior volume, and this can have a major impact on the feasibility and quality of the planned trajectories.

We aim to find efficient LTP algorithms that can both help avoid obstacle collision in realistic sensor-based obstacle detection scenarios, *and* optimize the trajectory for the landing site search task. In II we formulate the problem and optimization criteria, in III we describe the algorithms that were evaluated, and in IV evaluation results are presented.

II. PROBLEM FORMULATION

A. Landing site search process

The main motivation for this paper is the probabilistic multi-resolution approach for finding a suitable landing spot introduced by Pinkovich et al. in [16]. In that work, a search is conducted by calculating a feasible global flight path at a given altitude using prior information. The global path is such that a look-down camera installed on the UAV captures images from areas with high a-priori probability of being suitable for landing. An “Oracle” module then uses the images to calculate a post-priori probability map of the imaged area. Clearly, this requires that the flight path be executed safely by avoiding the collision with obstacles. Once probabilities have been updated, the UAV is lowered to a new altitude and a global path is recomputed. The process continues iteratively until a pre-specified threshold of suitability for landing has

All authors are with *The Henry and Marilyn Taub Faculty of Computer Sciences, Technion - Israel Institute of Technology, Haifa, Israel.*
yossimag@alumni.technion.ac.il,
ehudr@cs.technion.ac.il,
hector@ee.technion.ac.il

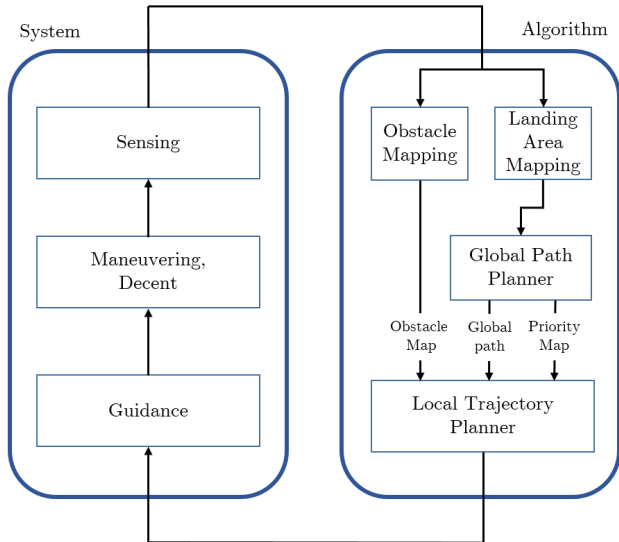


Figure 1: System diagram of the autonomous landing process.

been exceeded, or else failure is declared. Fig. 1 demonstrates this iterative process.

For simplicity, we assume the UAV can be considered to be a 3D point (meaning the configuration space is identical to the work space), and that it has no kinematic constraints. The flight path execution is computed by the LTP using two main outputs from the Global Path Planner (GPP): 1) A set of 3D points (or *way-points*) $\{\vec{r}_{G,k}\}$ specifying the desired global path, and 2) a 2D priority map $p_l(x, y)$ prioritizing flight over the different areas on ground (see Fig. 5). The higher the priority of a point (x, y) , the more likely it is for the look-down camera to take an image of a good landing spot beneath that point. The LTP has to optimize the actual flight trajectory using three optimization criteria: 1) The trajectory has to be as close as possible to the global path; 2) Maximize the average priority along the trajectory, and 3) Obstacle collision must be avoided. At each time instant, an initial point $\vec{r}_{init}(t)$ and a goal point $\vec{r}_{goal}(t)$ are defined for the LTP. Note that \vec{r}_{init} can be either the current or a previous position of the UAV, and $\vec{r}_{goal} = \vec{r}_{G,k}$ is the next global path point to be reached. If $\vec{r}_{G,k}$ is reached or found to be unreachable, it is removed from the way-point list and a local trajectory is planned to the next global point $\vec{r}_{goal} = \vec{r}_{G,k+1}$.

B. Obstacle detection and mapping

The UAV is assumed to be equipped with at least one or more sensors designed for the specific task of obstacle detection. Such sensors can be LiDAR, Radar, depth camera, or regular front-looking camera. The detection data of each one of the sensors is given at its own local coordinate system, usually polar and centered around its installation point and direction. For enabling obstacle global mapping, detection coordinates are transformed to a global coordinate system that coincide with the one used for navigation. Navigation data

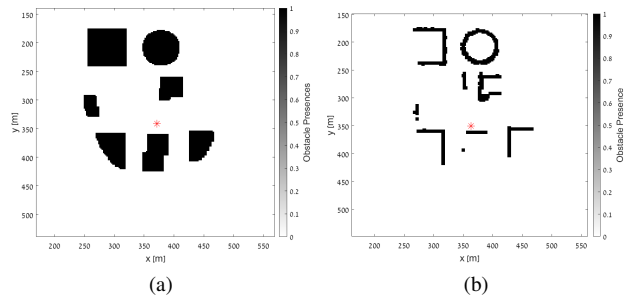


Figure 2: The obstacle map is always kept centered around the position of the UAV, indicating obstacle presence. A slice of the 3D map is shown for height $z = 50m$. The maximal detection range was set to be $100m$ in this case. (a) Volume sensing. (b) Surface sensing.

including UAV 3D position and orientation is assumed to be perfect.

The information regarding location of obstacles is concentrated in a 3D obstacle map (see Fig. 2). Because of memory consumption and run-time performance considerations, each cell in the obstacle map must have a limited resolution in every axis, and the whole map coverage must also be limited. Due to the coverage limitation, the map is kept centered around the position of the aircraft and shifted constantly for that purpose. Once the obstacle map is updated with the most current locations of obstacles, it serves as an input for trajectory planning.

For future reference, let C_{free} and C_{obs} be the subsets free and occupied by mapped obstacles, respectively. Let also C_{reach} be the reachable space, meaning the set of all points that can be connected to \vec{r}_{goal} by a trajectory $\vec{\ell} \in C_{free}$ of finite length.

C. Surface sensing and hollow obstacles

When sensors detect an obstacle they usually can only sense the outer surface of the obstacle but not its inner volume. The inner volume of the obstacle can never be reached by the sensors, so unless prior knowledge of its existence is given it is always falsely mapped to C_{free} by default. This surface sensing challenges the LTP, especially in cases when a global path point falls inside an obstacle. In these cases only trajectory planning failure can indicate a problem in the global path point (see Fig. 4). The local trajectory planning algorithm must therefore be complete so to reject invalid global path points, but avoid rejecting valid global path points that are in C_{reach} .

D. Optimization criteria

For optimizing the local trajectory ℓ between \vec{r}_{init} and \vec{r}_{goal} we define a penalty function $\varepsilon_p(\ell)$ to be minimized that has three main components:

- 1) **Obstacle avoidance** - The penalty for passing through an obstacle must be very high:

$$\varepsilon_{p0}(\ell) = \begin{cases} \infty, & \ell \text{ crosses an obstacle} \\ 0, & \text{otherwise} \end{cases} \quad (1)$$

- 2) **Minimal trajectory length** - The trajectory should be as short as possible for saving energy and time. The shortest path between \vec{r}_{init} and \vec{r}_{goal} is $L_{direct} = \|\vec{r}_{goal} - \vec{r}_{init}\|$. A suitable penalty function is a one proportional to the trajectory length L :

$$L = \int_{\vec{r}_{init}}^{\vec{r}_{goal}} d\ell \quad (2)$$

To avoid dependency on the absolute trajectory length, a proper penalty factor is therefore:

$$\varepsilon_{p1} = \frac{L}{L_{direct}} \quad (3)$$

Notice that L is always longer than L_{direct} , so the minimal penalty ε_{p1} will be 1 for $L = L_{direct}$.

- 3) **Prioritizing flight over certain areas** - Using the priority map given by the global path planner, $0 \leq p_l(x, y) \leq 1$, an additional term is added to the penalty function that reflects the average priority of regions covered beneath the flight trajectory:

$$\varepsilon_{p2} = -\frac{\int_{\ell} p_l(x, y) d\ell}{L} \quad (4)$$

The higher the average priority on the trajectory, the lower will be the penalty. Notice that $-1 \leq \varepsilon_{p2} \leq 0$, with minimal penalty of $\varepsilon_{p2} = -1$ when $p_l(x_\ell, y_\ell) = 1$ for all points on the trajectory.

The total penalty is set as a weighed combination of the three penalty functions:

$$\varepsilon_p(\ell) = \varepsilon_{p0}(\ell) + W_L \cdot \varepsilon_{p1} + W_p \cdot \varepsilon_{p2} \quad (5)$$

with W_L , W_p being some weighting constants that reflect the preference between the different optimization criteria. This optimization criterion resembles the risk function in [18], but instead of risk it takes into account look-down camera coverage for landing site search. ε_{p1} and ε_{p2} can alternatively be set as two separate cost function for bi-objective path planning algorithms such as BOA* [8].

III. LOCAL TRAJECTORY PLANNING

A. Trajectory planning using Bézier curves

A possible way of finding an optimal trajectory between \vec{r}_{init} and \vec{r}_{goal} is by using a cubic Bézier curve with four control points, $\vec{\ell}(s|\{P_n\})$, $n = 0, 1, 2, 3$. P_n are the control points, and s is the parameterization of the curve satisfying $0 \leq s \leq 1$.

$$\begin{aligned} \vec{\ell}(s|\{P_n\}) &= ([x_\ell(s), y_\ell(s), z_\ell(s)] | \{P_0, P_1, P_2, P_3\}) \\ &= (1-s)^3 P_0 + 3(1-s)^2 s P_1 + 3(1-s) s^2 P_2 + s^3 P_3 \end{aligned} \quad (6)$$

The first and last control points (P_0 and P_3) are set as \vec{r}_{init} and \vec{r}_{goal} respectively. For $s = 0$ the trajectory begins at P_0 ,

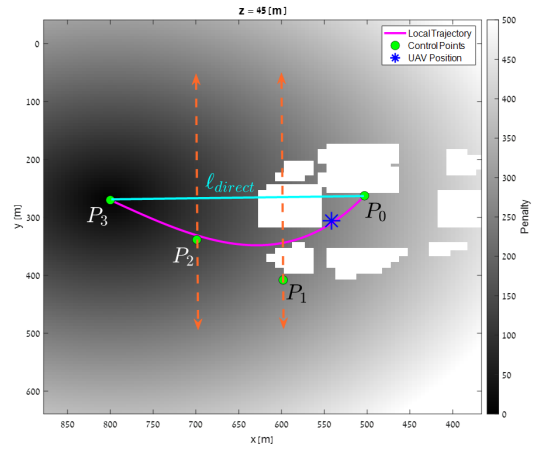


Figure 3: Local trajectory planning using a Bézier curve (magenta line) in a volume detection scenario. The Bézier control points (P_n) are marked in green, and the penalty map is shown at the background. Cells representing obstacle presence receive a high penalty. An exhaustive search is performed on points P_1 and P_2 , moving them along the dashed orange arrows that are perpendicular to the line ℓ_{direct} (in cyan). The optimal local trajectory is the one minimizing the cumulative penalty on the curve.

and for $s = 1$ the trajectory ends at P_3 . The search focuses on the middle control points, P_1 and P_2 , as to minimize ε_p :

$$(P_1^*, P_2^*) = \arg \min_{P_1, P_2} (\varepsilon_p) \quad (7)$$

P_1 and P_2 are initially set on line ℓ_{direct} connecting between P_0 and P_3 , spaced evenly between them as shown in Fig. 3. An exhaustive search is performed on P_1 and P_2 by moving both of them on the xy plane, in perpendicular direction to ℓ_{direct} . A main assumption is that change in height (movement in the z axis) is prohibited or is significantly limited to the very least. Nevertheless, to avoid singularity in some scenarios some limited search in the z axis of points P_1 and P_2 is also possible. If the search grid for P_1 and P_2 is of size M , then the complexity of the algorithm is $\mathcal{O}(M^2)$, and does not depend on resolution and coverage of the obstacle map.

B. Trajectory planning using Cost Wavefront Propagation

Finding a local trajectory using a polynomial method such as Bézier curves can succeed in simple cases, but can fail in more complicated scenarios such as narrow maze-like corridors or bug traps. A different solution for these scenarios is therefore required. One of the methods proposed for path planning is by calculating and following a navigation function [12]. A navigation function was generated by a Greedy Grid-based version of the cost Wavefront Propagation algorithm [2] (we name *GGWP*). In this algorithm the navigation function construction initiates from the goal point and propagates outward incrementally on the grid until reaching the initial point. At the second stage of the algorithm, after the initial point is reached, the shortest path is determined by following the geodesic line of the navigation function in a gradient

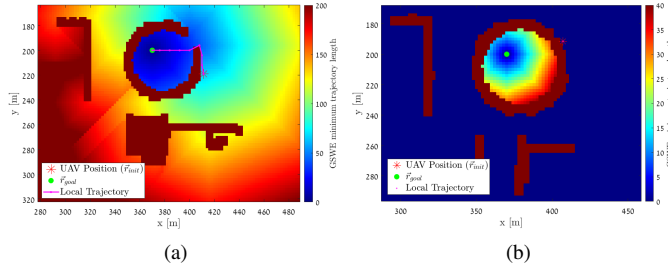


Figure 4: Greedy Grid-based Wavefront Propagation (GGWP) trajectory planning in surface detection scenarios where the goal point (green) falls inside an obstacle. (a) The surface of obstacle is not entirely detected and a path is calculated to the goal point. (b) The surface of the obstacle is entirely mapped and wavefront propagation is limited only to the interior volume of the obstacle. In this case planning failure is declared.

decent manor. The GGWP algorithm is able to find trajectories for complicated scenarios such as bug-traps (see Fig. 4) in $\mathcal{O}(N)$ (N being the number of cells in the occupancy map). However, it aims to only find short trajectories and cannot optimize for the landing site search problem in (5).

C. Trajectory planning using Length-Priority A^*

For minimizing ε_p on the trajectory the well known backwards weighted A^* algorithm [5, 13] was used. A graph is constructed by connecting all neighbouring samples in the regular grid of the obstacle map, and a trajectory search is performed on the graph edges. Similar to *riskA** [17], we also modify the cost-to-go function $g(\vec{r}_i, \vec{r}_{goal})$ and heuristic estimated cost-to-come function $h(\vec{r}_{init}, \vec{r}_i)$ of A^* , but in a way that supports the length-priority optimization of the trajectory:

$$g(\vec{r}_i, \vec{r}_{goal}) = \varepsilon_p(\ell : \vec{r}_i \rightarrow \vec{r}_{goal}) \quad (8)$$

$$h(\vec{r}_{init}, \vec{r}_i) = \frac{\|\vec{r}_{init} - \vec{r}_i\|}{L_{direct}} \quad (9)$$

$$f(\vec{r}_i, \vec{r}_{goal}) = g(\vec{r}_i, \vec{r}_{goal}) + W_{A^*} \cdot h(\vec{r}_{init}, \vec{r}_i) \quad (10)$$

with W_{A^*} the weighting factor of the heuristic function, and $f(\vec{r}_i, \vec{r}_{goal})$ the estimated total cost function. We name this form of weighted A^* algorithm *Weighted Length-Priority A^** , or *WLP- A^** . When setting $W_{A^*} = 1$ the algorithm becomes a form of A^* we name *Length-Priority A^** , or *LP- A^** . When setting $W_{A^*} = 0$ the algorithm becomes a form of the backwards Dijkstra algorithm we name *Length-Priority Dijkstra*, or *LP-Dijkstra*.

IV. RESULTS

A simulation of an autonomous flying UAV was implemented using Matlab. AirSim simulator [19] was used both for creating a Digital Surface Model (DSM) data of an urban area, for simulating obstacles and their detections, and for generating segmentation masks of elements on the ground and thus priority maps. The priority maps were calculated in two ways: 1. A *binari* map was created by setting a constant

value 1 in valid landing regions and 0 in invalid ones; 2. By running a Low-Pass Filter (*LPF*) on the segmentation mask, with a window size similar to the look-down camera footprint. The footprint size is given by $2h \cdot \tan(FOV/2)$, where the camera Field-Of-View (FOV) used was $53^\circ \times 53^\circ$ and h is the UAV height changing dynamically. For 50m height the camera footprint is approximately $50m \times 50m$. For testing the capability of obstacle avoidance, an artificial global path was used running intentionally through buildings. A statistical analysis was performed on such 50 randomly chosen linear global paths, all having length of 500m. The designated flight velocity was 3 m/sec. Different weights W_L, W_P were used for the penalty function. Obstacle detection by surface sensing of LiDAR rays was simulated at maximal range of 50m. The obstacle map grid (x, y, z) was of size $(200, 200, 40)$ ($N = 1.6 \cdot 10^6$ cells) and of resolution $(2m, 2m, 4m)$ (total map coverage of $(400m, 400m, 160m)$). The different priority maps and global paths used for the analysis are shown in In Fig 5, and in Fig. 6 an example is shown for the final trajectories, laid over the DSM and over the priority map.

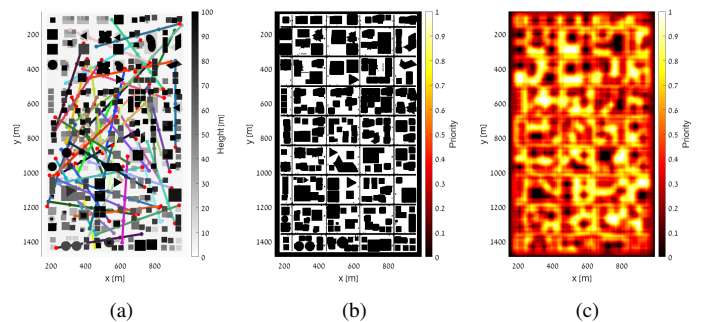


Figure 5: Statistical analysis for two different priority maps and 50 global paths. In (a) 50 linear global paths chosen randomly are placed on top of the DSM. All of the global paths were set at 50 m height. The red dots mark the starting points of each path. In (b) an (c) two different priority maps used for the analysis. Map (b) is *binari* having the value 1 above valid landing sites. In map (c) low-pass filtering (*LPF*) was applied for better representing the down-looking camera coverage beneath each location.

The parameters for evaluation were the average priority on the trajectory (\bar{P}), the average length ratio between the trajectory and the global path ($\frac{L_{LP}}{L_{GP}}$), and algorithm runtime. Run-time testing was performed on an Intel® Core™ i7-7820HQ CPU @ 2.90GHz machine with 16 GB RAM. Four algorithms were tested and compared: LP-Dijkstra, LP- A^* , WLP- A^* with $W_{A^*} = \sqrt{3}$ and GGWP. The reason for choosing $W_{A^*} = \sqrt{3}$ was for better comparison of WLP- A^* with GGWP, since both their path lengths are upper bounded by a $\sqrt{3}$ factor from the shortest path length on the grid.

Table I summarize the results of trajectory planning statistics using different algorithms and in the case of surface sensing and binaric priority map (in the parentheses are standard deviations). As expected, LP-Dijkstra gave the best results for average priority and total trajectory length, given

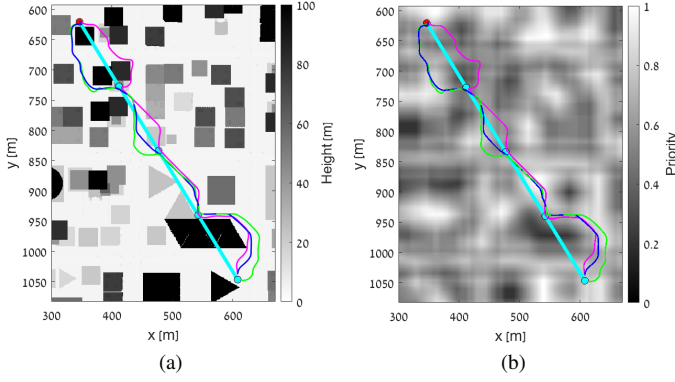


Figure 6: Local trajectory planning and execution using LP-Dijkstra in an urban environment. The different trajectories are laid over a DSM (a) and over a LPF priority map (b). The global path is marked in dotted cyan line, running at a height of $50m$, beginning from the top left corner (red point). Three planned trajectories are shown for different penalty functions: $W_P/W_L = 0$ (magenta), $W_P/W_L = 2$ (blue), $W_P/W_L = 5$ (green).

Table I: Comparison of different trajectory planning algorithms for binaric priority map. Best results are marked in red.

Algorithm	W_L	W_P	\bar{P}	$\frac{\overline{L_{LP}}}{L_{GP}}$	Average Run-time [msec]
LP-Dijkstra	1	0	0.61 (0.11)	1.25 (0.23)	20
LP-Dijkstra	0.5	1	0.82 (0.06)	1.34 (0.26)	20
LP- A^*	1	0	0.62 (0.11)	1.25 (0.23)	3.6
LP- A^*	0.5	1	0.76 (0.09)	1.37 (0.28)	3.6
WLP- A^* ($W_{A^*} = \sqrt{3}$)	1	0	0.61 (0.1)	1.26 (0.25)	2.5
WLP- A^* ($W_{A^*} = \sqrt{3}$)	0.5	1	0.66 (0.12)	1.4 (0.33)	2.5
GGWP	1	0	0.59 (0.12)	1.26 (0.21)	8.4

the proper optimization weights. However, it also had the slowest run-time. Different W_P/W_L ratios were tested to determine what is a good operating point (Fig. 7). For small W_P/W_L ratios short trajectories were generated with poor average priority values. For large W_P/W_L ratios the algorithm focused on improving the average priority, even at the price of significantly increasing the average trajectory length and dispersion. A good operating point was found to be $W_P/W_L = 2$, improving average priority by $\sim 34\%$ to 0.82 while elongating the trajectory by only $\sim 7.2\%$ on average relative to the $W_P/W_L = 0$ operating point. The shortest run-time was measured for WLP- A^* . GGWP generated trajectories only 0.8% longer on average than LP-Dijkstra for $W_P = 0$, and of similar average length compared to WLP- A^* with $\sqrt{3}$ weighting factor.

Table II summarize the results when using a LPF priority map for the operating point $W_P/W_L = 2$. In this case the differences in performance between the different algorithms

Table II: Comparison of different trajectory planning algorithms for LPF priority map.

Algorithm	W_L	W_P	\bar{P}	$\frac{\overline{L_{LP}}}{L_{GP}}$
LP-Dijkstra	0.5	1	0.68 (0.12)	1.28 (0.24)
LP- A^*	0.5	1	0.65 (0.1)	1.27 (0.29)
WLP- A^* ($W_{A^*} = \sqrt{3}$)	0.5	1	0.59 (0.12)	1.26 (0.21)

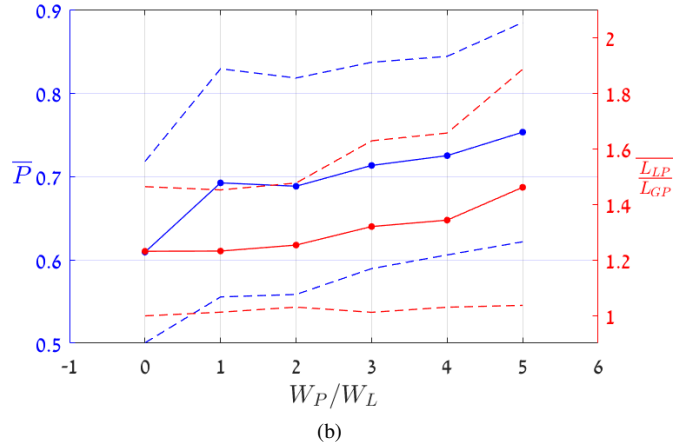
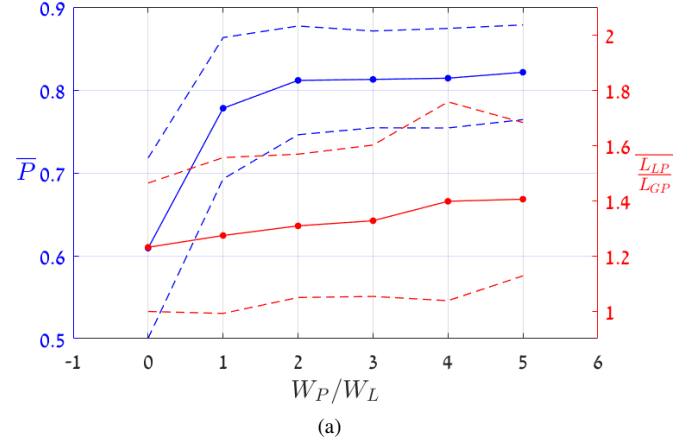


Figure 7: LP-Dijkstra performance for different W_P/W_L ratios using a binaric (a) and LPF (b) priority maps. The dashed lines are standard deviation margins.

are significantly reduced due to the spatial averaging nature of the low-pass filtering. Now in order to find a trajectory that has higher average priority, more significant spatial changes have to be made to the trajectory. These significant changes forces the trajectory to become longer and results in higher penalty. The priority improvement are therefore less favoured.

V. CONCLUSION AND FUTURE WORK

The autonomous landing capability is important for increasing autonomy of UAVs. The landing mission requires a unique planning optimization process including a suitable local

trajectory planning that can assist the mission while avoiding obstacle collision. The main contributions of this work is the introduction of a new optimization criterion and analysis methodology for trajectory planning, using a pre-planned global path and a priority map of landing site search regions on the ground. Algorithms were developed and evaluated using a simulation of real-life scenarios where only the surface of obstacles are detectable, and only at close enough distance. Trajectory planning using polynomial methods such as Bézier curves may fail in such cases of surface sensing. We introduce and evaluate the performance of a weighted A^* algorithm modified with the new optimization criterion (namely WLP- A^*). A greedy grid-based version of the cost wave propagation path planning algorithm (namely GGWP) was also evaluated and was shown to work well in practice for calculating short trajectories. Simulations show that in addition to finding feasible trajectories that avoid collisions with obstacles, our optimization process can significantly increase the probability of finding a proper landing site.

However, in this work the UAV navigation data was assume to be perfect with no errors what so ever. The impact of navigation errors on obstacle mapping and consequently on trajectory planning may be profound, and therefore must also be included in future evaluations. The influence of other important parameters such as sensor detection range and mapping resolution must also be examined.

REFERENCES

- [1] R. Cimurs and I.H. Suh. “Time-optimized 3D Path Smoothing with Kinematic Constraints”. In: *Int. J. Control Autom. Syst.* 18 (2020), pp. 1277–1287.
- [2] Leo Dorst and Karen Trovato. “Optimal Path Planning By Cost Wave Propagation In Metric Configuration Space”. In: *Mobile Robots III*. Ed. by William J. Wolfe. Vol. 1007. International Society for Optics and Photonics. SPIE, 1989, pp. 186–197. DOI: 10.1117/12.949097. URL: <https://doi.org/10.1117/12.949097>.
- [3] T. Elmokadem. “Real-time Safe Navigation Strategy for Mobile Robots in 3D:A Deforming Path Approach”. In: *2019 Chinese Control Conference (CCC)*. 2019, pp. 3833–3838.
- [4] Fei Gao et al. “Teach-repeat-replan: A complete and robust system for aggressive flight in complex environments”. In: *IEEE Transactions on Robotics* (2020).
- [5] Eric A Hansen and Rong Zhou. “Anytime heuristic search”. In: *Journal of Artificial Intelligence Research* 28 (2007), pp. 267–297.
- [6] P. E. Hart, N. J. Nilsson, and B. Raphael. “A Formal Basis for the Heuristic Determination of Minimum Cost Paths”. In: *IEEE Transactions on Systems Science and Cybernetics* 4.2 (1968), pp. 100–107. DOI: 10.1109/TSSC.1968.300136.
- [7] Mojtaba Hedayatpour, Mehran Mehrandezh, and Farokh Janabi-Sharifi. “Path Planning and Controlled Crash Landing of a Quadcopter in case of a Rotor Failure”. In: *arXiv preprint arXiv:1809.09334* (2018).
- [8] Carlos Hernández Ulloa et al. “A Simple and Fast Bi-Objective Search Algorithm”. In: *Proceedings of the International Conference on Automated Planning and Scheduling* 30.1 (June 2020), pp. 143–151.
- [9] Y. Hu et al. “Path Planning of UGV Based on Bézier Curves”. In: *Robotica* 37.6 (2019), pp. 969–997. DOI: 10.1017/S026357471800139X.
- [10] Bryce T Ingersoll et al. “UAV path-planning using Bezier curves and a receding horizon approach”. In: *Aiaa modeling and simulation technologies conference*. 2016, p. 3675.
- [11] Ishay Kamon, Elon Rimon, and Ehud Rivlin. “TangentBug: A Range-Sensor-Based Navigation Algorithm”. In: *The International Journal of Robotics Research* 17.9 (1998), pp. 934–953. DOI: 10.1177/027836499801700903. URL: <https://doi.org/10.1177/027836499801700903>.
- [12] S. M. LaValle. *Planning Algorithms*. Available at <http://planning.cs.uiuc.edu/>. Cambridge, U.K.: Cambridge University Press, 2006.
- [13] Maxim Likhachev, Geoffrey J Gordon, and Sebastian Thrun. “ARA* : Anytime A* with Provable Bounds on Sub-Optimality”. In: *Advances in Neural Information Processing Systems*. Ed. by S. Thrun, L. Saul, and B. Schölkopf. Vol. 16. MIT Press, 2004. URL: <https://proceedings.neurips.cc/paper/2003/file/ee8fe9093fbbb687bef15a38facc44d2-Paper.pdf>.
- [14] S. Lin, X. Kong, and L. Liu. “Development of an intelligent UAV path planning approach to minimize the costs in flight distance, time, altitude, and obstacle collision”. In: *2019 19th International Symposium on Communications and Information Technologies (ISCIT)*. 2019, pp. 238–243.
- [15] K.N. McGuire, G.C.H.E. de Croon, and K. Tuyls. “A comparative study of bug algorithms for robot navigation”. In: *Robotics and Autonomous Systems* 121 (2019), p. 103261. ISSN: 0921-8890. DOI: <https://doi.org/10.1016/j.robot.2019.103261>. URL: <https://www.sciencedirect.com/science/article/pii/S0921889018306687>.
- [16] Barak Pinkovich et al. “Finding a Landing Site on an Urban Area: A Multi-Resolution Probabilistic Approach”. Submitted for publication. 2021.
- [17] S. Primatesta et al. “A Risk-based Path Planning Strategy to Compute Optimum Risk Path for Unmanned Aircraft Systems over Populated Areas”. In: *2020 International Conference on Unmanned Aircraft Systems (ICUAS)*. 2020, pp. 641–650. DOI: 10.1109/ICUAS48674.2020.9213982.
- [18] Stefano Primatesta, Giorgio Guglieri, and Alessandro Rizzo. “A risk-aware path planning strategy for UAVs in urban environments”. In: *Journal of Intelligent & Robotic Systems* 95.2 (2019), pp. 629–643.
- [19] Shital Shah et al. “Airsim: High-fidelity visual and physical simulation for autonomous vehicles”. In: *Field and service robotics*. Springer. 2018, pp. 621–635.